THE JOURNAL OF PHYSICAL CHEMISTRY A

pubs.acs.org/JPCA Article

Spectral Tuning and Photoisomerization Efficiency in Push−Pull Azobenzenes: Designing Principles

Flavia Aleotti,[‖] Artur Nenov,[‖] Luca Salvigni, Matteo Bonfanti, Mohsen M. El-Tahawy, Andrea Giunchi, Marziogiuseppe Gentile, Claudia Spallacci, Alessia Ventimiglia, Giuseppe Cirillo, Lorenzo Montali, Stefano Scurti, Marco Garavelli,* and Irene Conti*

Cite This: *J. Phys. Chem. A* 2020, 124, 9513−9523 Read Online

ACCESS | Metrics & More | Article Recommendations | Supporting Information

ABSTRACT: This work demonstrates how *push−pull* substitution can induce spectral tuning toward the visible range and improve the photoisomerization efficiency of azobenzene-based photoswitches, making them good candidates for technological and biological applications. The red-shifted bright $\pi\pi^*$ state (S_2) behaves like the lower and more productive dark $n\pi^*$ (S_1) state because less potential energy along the planar bending mode is available to reach higher energy unproductive $n\pi^*/S_0$ crossing regions, which are responsible for the lower quantum yield of the parent compound. The stabilization of the bright $\pi\pi^*$ state and the consequent increase in isomerization efficiency may be regulated *via* the strength of *push−pull* substituents. Finally, the torsional mechanism is recognized here as the unique productive route because structures with bending values attributable to the inversion mechanism were never detected, out of the 280 $\pi\pi^*$ time-dependent density functional theory (RASPT2-validated) dynamics simulations.

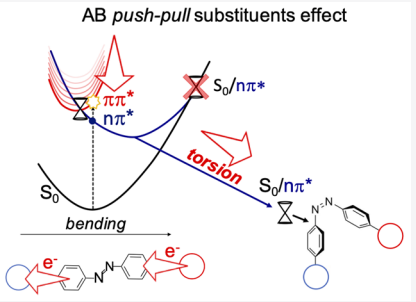

INTRODUCTION

Azobenzene (AB) is a prototypical photoresponsive molecule undergoing a reversible photoinduced isomerization between its *cis* and *trans* configurations, which is strongly attractive for a widespread range of applications. The *trans* ↔ *cis* interconversion mechanism has been debated for a long time:[1−10] it could take place through rotation around the central double bond (*torsion*) or through an in-plane *bending* motion (Scheme 1). Eventually, hybrid *torsion-bending* processes were recently proposed.[11−14] Interestingly, the well-separated absorption wavelengths of the two isomers make this molecule suitable for optical switches in technological[15−17] or biological[18−20] devices and in the development of light-powered molecular machines.[2,3,21−27] Both isomers show two absorption bands in the UV−vis window: the more intense one is associated to a $\pi \rightarrow \pi^*$ transition, peaking in the UV region (301/265 nm in the gas phase, *trans*/*cis*, respectively[28]), while the much weaker band in the visible range (440/425 nm[28]) is associated to a symmetry-forbidden $n \rightarrow \pi^*$ transition. These $\pi\pi^*/n\pi^*$ bands are separated enough to allow their selective irradiation: interestingly, excitation in the UV ($\pi\pi^*$) and in the visible region ($n\pi^*$) shows significantly different quantum yields (QYs), about 11% and 25%, respectively, in the *trans* case and 27% and 56% in the *cis* case in *n*-hexane.[29] The QY wavelength dependence, which is in contrast with Kasha's rule, suggests that different reaction mechanisms may take place starting from the $\pi\pi^*$ or $n\pi^*$ excited states (ESs),[12] an issue that is still under discussion in experimental[8,30] and theoretical[8,11,31−33] studies. Because of the reversibility of the isomerization, its speed, and the simplicity of incorporating azobenzene in complex structures, many studies are focused on red-shifting the intense $\pi\pi^*$ bands, whose UV absorption is limiting technological and biological applications. For this purpose, *push−pull* substituents have demonstrated to be good candidates:[37−40] the simultaneous destabilization of the last π orbital (electron-donating substituent) and stabilization of the

Scheme 1. Possible Isomerization Mechanisms

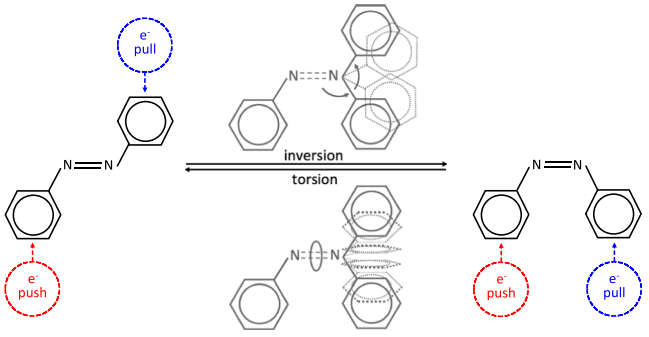

Received: September 23, 2020
Published: November 10, 2020

https://dx.doi.org/10.1021/acs.jpca.0c08672
J. Phys. Chem. A 2020, 124, 9513−9523

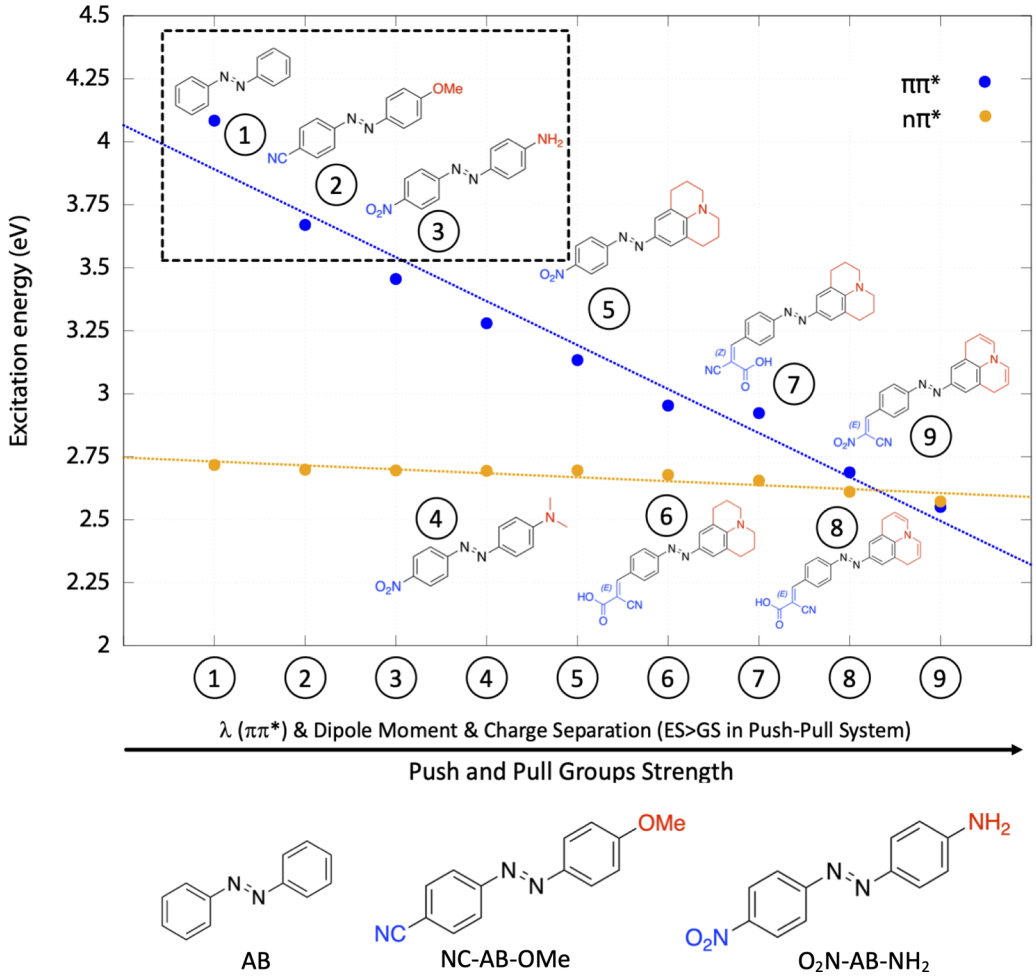

Figure 1. Selected AB-systems (bottom) considering an ensemble of eight *push*−*pull* derivatives: correlation between the strength of *push*−*pull* substituents and the lowest nπ^*/$\pi\pi^*$ vertical excitation energies (yellow/blue lines, respectively).

π^* LUMO (electron-withdrawing substituent), results in red shift of the $\pi\pi^*$ absorption,[8,18,33,41−46] which influences the $\pi\pi$−nπ^* energy gap and leads to a change in the photoisomerization properties. The aim of this work is to evaluate how *push*−*pull* substituents could control the capability of AB-based photoswitches, tuning the linear absorption energy and the isomerization efficiency, depending on the mechanism behind. For this purpose, we compare the behavior of the parent AB with two different *push*−*pull*-substituted systems with increasing electron-donating/withdrawing strength: 4-methoxy-4′-cyanoazobenzene (NC−AB−OMe) and 4-(4-nitrophenylazo)aniline (O_2N−AB−NH_2, also known as Disperse Orange 3 or DO3); see Figure 1. The comparison is made by means of time-dependent density functional theory (TD-DFT) semiclassical dynamics simulations (RASPT2-validated at crossing points, see Table S11) accounting for multireference dynamically correlated energies. The results allow us to identify the *control knobs* of productive (*i.e.*, photoisomerization) *versus* nonproductive (*i.e.*, aborted photoisomerization) radiationless decays, thus paving the way to a rational design of AB derivatives with tuneable spectral properties and increased photoisomerization efficiency.

RESULTS AND DISCUSSION

Comparison between AB and the two *push*−*pull*-substituted systems NC−AB−OMe and O_2N−AB−NH_2 (Figure 1) was done by conducting mixed quantum−classical dynamics simulations at the TD-DFT/CAM-B3LYP/6-31G* level, following 40 gas-phase trajectories on both the *cis* and *trans* isomer of the three systems (240 trajectories in all), initiated on the bright $\pi\pi^*$ state. Nonadiabatic events were treated with a simplified hopping scheme, relying on the energy gap as a criterion for changing the electronic state, fixed lower than 3 kcal/mol. Back hopping was always allowed between ESs, while it was not permitted once the trajectory decayed on the ground state (GS). We ran 40 additional trajectories on the *trans*-AB nπ^* state that were employed as a reference for the photobehavior of the more productive dark state in the parent compound. TD-DFT/CAM-B3LYP/6-31G* was validated by benchmarking against RASPT2 static calculations at the S_1/S_0 crossing points, using an accurate setup that was previously tested for the parent system (MS-RASPT2/RASSCF/ANO-L-VDZP),[12,47] where the active space (including the valence π-orbitals and the nitrogen lone pairs) was appropriately enlarged for the *push*−*pull*-substituted systems (Figures S1−S3 in the Supporting Information). However, because TD-DFT fails to produce correctly shaped potential energy surfaces (PESs) in the region surrounding intersections with S_0, we limit our analysis to the ES dynamics until the S_1/S_0 gap is lower than 3 kcal/mol (S_1/S_0 crossing seam). The O_2N−AB−NH_2 and NC−AB−OMe derivatives were selected after a preliminary study (at the CAM-B3LYP/6-31G* level) of eight

https://dx.doi.org/10.1021/acs.jpca.0c08672
J. Phys. Chem. A 2020, 124, 9513−9523

Table 1. Experimental, TD-DFT/CAM-B3LYP/6-31G*, and MS-RASPT2/SA-8-RASSCF/ANO-L-VDZP Vertical Excitation Energies (Oscillator Strengths in Parentheses) and Excited-State Lifetimes (τ) of *trans*- and *cis*-AB, NC−AB−OMe, and O_2N−AB−NH_2 in the Gas Phase[a]

		excitation energy $\pi\pi^*$				excitation energy $n\pi^*$				τ (fs)	
		trans		*cis*		*trans*		*cis*			
		nm	eV	nm	eV	nm	eV	nm	eV	*trans*	*cis*
AB	exp. value	301[28]	4.12	265[28]	4.68	440[28]	2.82	425[28]	2.92	170, 420[5]	200[b,34]
	TD-DFT	304	4.08 (0.82)	265	4.69 (0.18)	456	2.72 (0.00)	464	2.67 (0.03)	168, 231, 323 (tors. path)	242, 278
	RASPT2	322	3.85 (0.42)	302	4.11 (0.05)	478	2.59 (0.00)	450	2.75 (0.02)	–	–
NC−AB−OMe	exp. value[c]	380[35]	3.26	–		460[35]	2.70	–		–	–
	TD-DFT	338	3.67 (1.10)	288	4.30 (0.40)	459	2.70 (0.00)	472	2.62 (0.05)	70, 225, 386 (tors. path)	181, 221
	RASPT2	342	3.62 (0.60)	322	3.85 (0.15)	509	2.44 (0.00)	474	2.62 (0.05)	–	–
O_2N−AB−NH_2	exp. value	353[36]	3.51	–		442[36]	2.81	–		–	–
	TD-DFT	359	3.46 (1.10)	313	3.96 (0.35)	460	2.70 (0.00)	472	2.62 (0.07)	86, 227, 300 (tors. path)	118, 144
	RASPT2	414	2.99 (0.84)	348	3.56 (0.15)	453	2.74 (0.00)	506	2.45 (0.05)	–	–

[a]Optimized GS *bending* and *torsional* parameters are shown at the top of Figures 2 and 4 (Cartesian coordinates for the *trans* and *cis* conformers are given in the Supporting Information). Details on the S_2 and S_1 average lifetimes, calculated on all trajectories or separately on the *torsional* or *bending* paths, are documented in Tables S4−S6, respectively. [b]In ethanol at room temperature. [c]In 2-methyltetrahydrofuran (MTHF) at 77 K.

systems with increasing *push*−*pull* strength: Figure 1 clearly shows how the substituents red-shift the $\pi\pi^*$ state, leaving the dark $n\pi^*$ roughly unchanged. Increasing the *push*−*pull* strength reduces the $\pi\pi^*/n\pi^*$ energy gap, until inversion of the $\pi\pi^*/n\pi^*$ energy order (Figure 1 and Table S1). Because of their small size, the selected systems are good candidates to make accurate predictions about these promising *push*−*pull* derivatives. The quantitative accuracy of the employed method is supported by the good agreement between the experimental and computed vertical energies for *trans*/*cis*-AB, *trans*-NC−AB−OMe, and *trans*-O_2N−AB−NH_2 (see Table 1). This also validates the prediction for the absorption values ($\pi\pi^*$ and $n\pi^*$), which are not available in the literature, in particular for the *push*−*pull cis*-conformers, which are thermally unstable and therefore difficult to isolate and characterize.[40] Besides stabilizing the $\pi\pi^*$ state, the growing strength of the *push*−*pull* substituents also affects the charge distribution on the two phenyl rings and, consequently, the molecular dipole moment (see Figure S4 and Table S1 in the Supporting Information). The charge separation is proportional to the electron-donating/withdrawing strength, as shown in Figure 1: $-NH_2$ is a better *push* group than −OMe because of the lower electronegativity of the nitrogen atom; at the same time, the $-NO_2$ substituent "*pulls*" more than the −CN. The charge excess on the two halves is notably larger on the bright $\pi\pi^*$ ES, with a consequent increase in the dipole moment value: 0.162/0.247 D and 0.241/0.327 D on $\pi\pi^*$ for *trans*/*cis* NC−AB−OMe and the O_2N−AB−NH_2, respectively, compared with 0.074/0.071 D and 0.115/0.106 D of the GS. The larger dipole moment of the *cis* conformer could be referred to the nonplanar geometry that hinders the orbital delocalization, leading to a larger charge separation between the two halves.

We show how the *push*−*pull* derivatives behave dynamically different, compared to the parent system, when they are excited to the bright $\pi\pi^*$ state in the following. Because photoexcited *trans*- and *cis*-isomers lead to quite different paths[11] (as demonstrated by the experimental lifetimes in Table 1), we will discuss them separately.

***trans*-AB Systems.** Looking at the S_2 dynamics leading to the initial $S_2 \rightarrow S_1$ decay, we notice that the CNNC dihedral angle stays close to 180° in all the systems, while the CNN bending angles close and then oscillate around a value that is a bit smaller than that in the FC geometry, in agreement with recent studies on the AB photoisomerization.[12] Figure 2 shows the normalized distribution of the CNNC torsion (top) and CNN bending (bottom) trajectories along the *trans*-dynamics of the three systems, including the $n\pi^*$ *trans*-dynamics of AB. The left panels refer to the dynamics on S_2 [panels (a−c) and (h−j)], while the right plots refer to the dynamics on S_1 after decay from S_2 [panels (e−g) and (l−n)] or after direct excitation [for *trans*-AB, panels (d,k)]. The most significant effect of *push*−*pull* substitution is a drastically shorter $\pi\pi^*$ lifetime with respect to the parent compound, where S_2 is living two times longer than in the substituted *trans*-systems (168 fs for AB against 70 and 86 fs for NC−AB−OMe and O_2N−AB−NH_2, respectively; see vertical dashed lines in Figure 2, left part).

On the other hand, in the subsequent dynamics on the $n\pi^*$ state (S_1), bending oscillations accompany the torsional motion (Figure 2, right part), leading to a $S_1 \rightarrow S_0$ crossing region spanning from planar to fully rotated CNNC values (Tables S4−S6 in the Supporting Information). This is due to an extended S_0/S_1 crossing seam, that has been extensively documented in previous studies,[11,47,48] covering both *bending* and *torsional* modes, where the fully (∼90°) rotated structures are the lowest in energy, but also, higher energy, less-rotated structures could be accessible through the bending mode, provided that enough kinetic energy is available in the dynamics. Based on the characteristics of the $S_1 \rightarrow S_0$ seam, we have grouped the trajectories in two different sets, labelled *torsional* and *bending paths*, based on the CNNC torsional value at the $S_1 \rightarrow S_0$ decay: the former includes trajectories decaying on S_0 at CNNC < 135° (half between 180 and 90°), the latter includes trajectories which, to a great extent, preserve the planarity of azobenzene until decaying to the GS (CNNC > 135°). Most trajectories for all the three *trans*-systems follow the *bending path* (82.5/65/65% for AB/NC−AB−OMe/

https://dx.doi.org/10.1021/acs.jpca.0c08672
J. Phys. Chem. A 2020, 124, 9513−9523

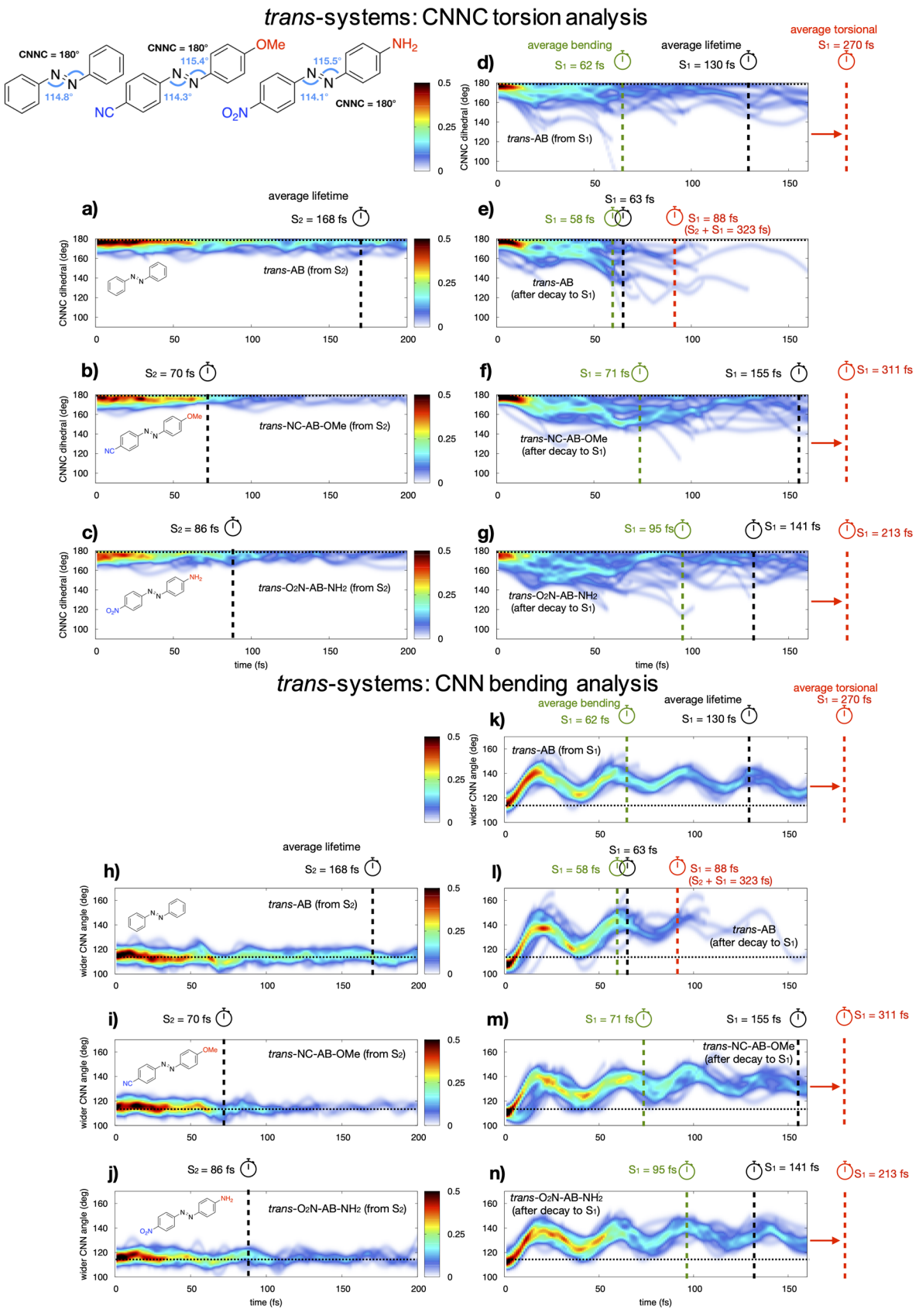

Figure 2. Normalized distribution of the CNNC *torsional* value (top panels) and widest CNN bending value (bottom panels) over time for the *trans*-system dynamics (40 for each panel) on S_2 (left) and on S_1 (right) until decay to the GS. The color scale refers to the normalized density of trajectories. The panels (d,k) refer to the 40 dynamics initiated in the $n\pi^*$ for *trans*-AB. Vertical dashed lines: ES lifetimes averaged over all trajectories (black) and over *torsional* (red) or *bending paths* (green). Horizontal dotted lines: FC value of the relative coordinate. Top left structures: CNNC torsion and CNN bending values in the S_0 minimum *trans*-systems (DFT/B3LYP/6-31G* optimized).

https://dx.doi.org/10.1021/acs.jpca.0c08672
J. Phys. Chem. A 2020, 124, 9513−9523

Table 2. Analysis of the Decay geometries[a]

		torsional path				*bending* path			
		AB		NC−AB−OMe	O_2N−AB−NH_2	AB		NC−AB−OMe	O_2N−AB−NH_2
		$\pi\pi^*$	$n\pi^*$	$\pi\pi^*$	$\pi\pi^*$	$\pi\pi^*$	$n\pi^*$	$\pi\pi^*$	$\pi\pi^*$
		Trans-Systems							
	relative amount (%)	17.5	32.4	35.0	35.0	82.5	67.6	65.0	65.0
$S_2 \rightarrow S_1$ hop	CNNC (deg)	173		177	173	175		176	173
	CNN−NNC (deg)	108−105		108−111	114−110	108−104		107−110	110−113
	N═N (Å)	1.40		1.39	1.32	1.40		1.36	1.32
$S_1 \rightarrow S_0$ hop	CNNC (deg)	126	119	123	123	157	156	161	158
	CNN−NNC (deg)	145−141	139−134	130−136	138−131	149−142	147−141	147−142	144−139
	N═N (Å)	1.24	1.24	1.28	1.28	1.24	1.23	1.23	1.23
		Cis-Systems							
$S_2 \rightarrow S_1$ hop	CNNC (deg)	12		14	14				
	CNN−NNC (deg)	127−113		131−112	131−120				
	N═N (Å)	1.43		1.39	1.26				
$S_1 \rightarrow S_0$ hop	CNNC (deg)	79		74	75				
	CNN−NNC (deg)	132−111		138−115	128−115				
	N═N (Å)	1.31		1.31	1.29				

[a]*Trans*-system dynamics: torsional path = CNNC < 135° at the S_1/S_0 decay and bending path = 135° < CNNC < 180° at the S_1/S_0 decay. The geometrical parameters are averaged over all the set of trajectories belonging to each *torsional*/*bending* group. *Cis*-system dynamics: all trajectories are ascribable to the *torsional* path (>99%), for which CNNC > 45° at the S_1/S_0 decay.

O_2N−AB−NH_2, respectively; see Table 2), but none of them reach bending values that could justify a possible *inversion*-driven isomerization process (*i.e.*, close to 180°; see Scheme 1, bottom part of Figure 2, and Tables S4−S6). This explains the smaller QY of *trans*-AB from $\pi\pi^*$ (11% vs 25% from $n\pi^*$[29]): the most populated bending paths are reaching S_0/S_1 CIs with neither *bending* nor *torsion* values large enough to allow the *trans*−*cis* isomerization. Moreover, the *bending* motions are mainly symmetric (see values in Tables S4−S6), and even a hypothetical concerted bending mechanism would lead back to the reagent. Consequently, on the basis of the large number of dynamics on the three *trans*-systems (120, 40 for each system), we conclude that the only productive process follows the *torsion* mechanism. However, because our analysis is limited to the ES dynamics until decay to the GS, we can only have an upper bound estimate of the $\pi\pi^*$ QY, which is given by the number of *torsional paths* populated for each system: we obtained 17.5%, 35%, and 35% for *trans*-AB, NC−AB−OMe, and O_2N−AB−NH_2, respectively, envisaging a larger QY in the *push*−*pull* systems than that in the parent AB (see Table 2). To prove that the isomerization QY correlates well with the population of the *torsion* mode, we ran 40 dynamics for *trans*-AB (using the same initial conditions as for the $\pi\pi^*$ state) starting from the more productive $n\pi^*$ state (experimental QY = 25%[29]): in this case, 32.4% of the trajectories belong to the *torsional* path (Table 2), a value that is close to the observed QY. Previous semiclassical dynamics by Granucci and Persico[49] employing a semiempirical Hamiltonian reported values for the QYs of 15% and 33% starting from the $\pi\pi^*$ and $n\pi^*$state, respectively, which is perfectly in line with the amount of torsional trajectories obtained in each case from our simulations. Remarkably, the ratio between the *torsional paths* populated when initiating the dynamics either in the $\pi\pi^*$ or $n\pi^*$ state (Table 2) matches well with the experimental $\pi\pi^*$ and $n\pi^*$ QY ratio (theoretical estimate: 17.5/32.4 = 0.54, experimental QY ratio in *n*-hexane:[29] 11/25 = 0.44). This strengthens the hypothesis that CN═NC torsion is the productive mechanism, which explains the larger QY in the *trans push*−*pull* systems.

To further support and rationalize that the *push*−*pull* systems could be more productive than the parent *trans*-AB because of the larger population of *torsional paths*, Figure 3 shows the $S_2 \rightarrow S_1$ (red) and the $S_1 \rightarrow S_0$ (dark blue) hopping point distribution, along the *bending*/*torsional* coordinates, for the $\pi\pi^*$ trajectories of the three different systems. Interestingly, for the *push*−*pull* systems, the $S_1 \rightarrow S_0$ hopping point distribution obtained starting from the bright $\pi\pi^*$ state is matching with the *trans*-AB distribution obtained starting from the more efficient $n\pi^*$ state [light-blue points in Figure 3 panel (a) *versus* blue points in panels (b,c)], envisaging that the *push*−*pull* derivatives excited to $\pi\pi^*$ behave exactly as AB excited to $n\pi^*$, for which a larger isomerization productivity is experimentally documented. Instead, the $S_1 \rightarrow S_0$ decay points for *trans*-AB when excited to S_2 show a clearly different distribution, largely concentrated in the *bending* region. Additionally, the average bending values at the $S_1 \rightarrow S_0$ hopping points are a bit smaller for the *torsional* trajectories (and in the $n\pi^*$ dynamics) than for the *bending* ones (see Table 2 and Figure 3), which is perfectly in line with the shape of the S_1/S_0 crossing region depicted in our earlier studies,[11] showing that fully rotated CIs (∼90°) display smaller bending values than less-rotated (and therefore less productive) ones.[11,47] It is thus apparent that by calibrating the strength of *push*−*pull* substituents, one could red-shift the absorption maximum of the bright $\pi\pi^*$ state, bringing it closer to that of the productive $n\pi^*$ and concurrently increase the photoisomerization efficiency, two main achievements in the design of photoactive AB-based systems.

Concerning the lifetimes, we see a nice agreement between experiments and theory: time-resolved photoelectron spectroscopy experiments[5] show two decay time constants for *trans*-AB: the shorter (170 fs) is perfectly matching our *trans*-AB $S_2 \rightarrow S_1$ average decay time value of 168 fs (black dashed line in Figure 2a,h and in Table 1); the longer one (420 fs) is close to the computed S_2 + S_1 average decay time of 323 fs of the

https://dx.doi.org/10.1021/acs.jpca.0c08672
J. Phys. Chem. A 2020, 124, 9513−9523

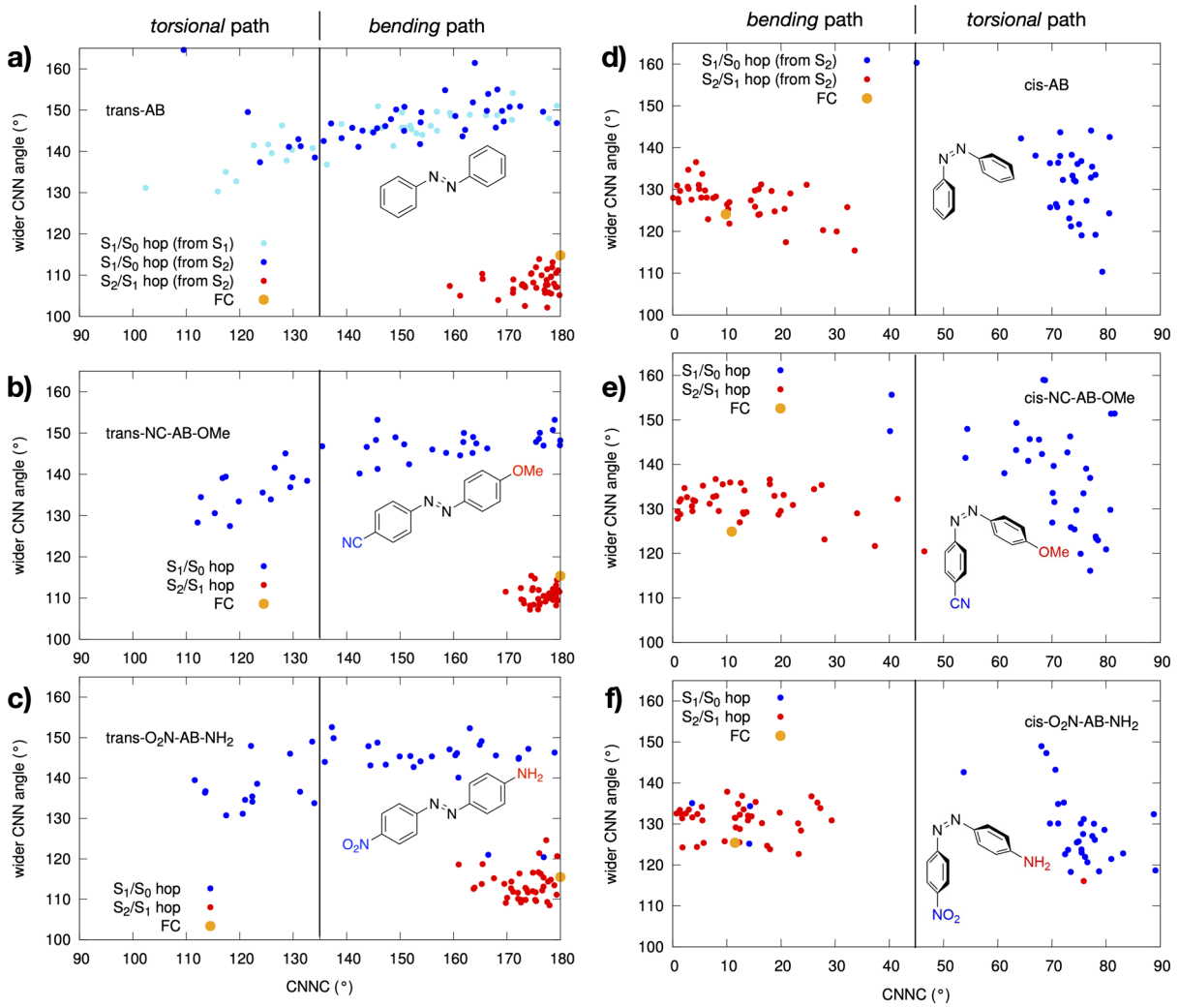

Figure 3. Projection of all the decay geometries in the *torsion/bending* space for the *trans* (left part) and *cis* (right part) dynamics. Red points = $S_2 \rightarrow S_1$, blue points = $S_1 \rightarrow S_0$ hopping point distribution populated along the $\pi\pi^*$ (S_2) dynamics of the three systems. Light-blue points in panel (a) correspond to $S_1 \rightarrow S_0$ hopping points populated by the 40 trajectories starting from the *trans*-AB $n\pi^*$ (S_1) state. The vertical line in each panel defines the *torsional* and the *bending* regions (i.e., half way between 180 and 90° for the *trans*-isomers and between 0 and 90° for the *cis* ones).

slower *torsional paths* (red dashed line in Figure 2e,l; see also Table 1 and details on average lifetimes in Table S4). Even though the original work[5] attributed the longer experimental lifetime of 420 fs to two higher lying $\pi\pi^*$ states (S_3–S_4), the low oscillator strength reported for them[5,11] suggests that the population of S_2 is by far more probable and that the 420 fs time constant could instead be associated to the S_2 + S_1 deactivation following the CNNC torsional motion toward the twisted S_1/S_0 crossing region. This hypothesis was already proposed by Granucci *et al.*,[49] and it is also supported by the following theoretical[50−52] and experimental[34] studies reporting a S_1 lifetime of about 0.4 ps.

An insight into the behavior of the dynamics following $S_2 \rightarrow S_1$ decay clearly shows an average $n\pi^*$ S_1 lifetime that is almost doubled in the *push−pull* derivatives than in AB (155 fs, 141 fs, and 63 fs for NC−AB−OMe, O_2N−AB−NH_2, and AB, respectively, black dashed lines in Figure 2e−g). Interestingly, the S_1 average lifetimes of the *push−pull* systems resemble those of the more productive dark $n\pi^*$ state of the parent AB when it is directly excited, (130 fs, see black dashed line in Figure 2d,k), once again showing that the dynamics of the *push−pull* systems excited to the $\pi\pi^*$ resembles that of the $n\pi^*$ state of AB. Eventually, we observe that the S_1 *torsional path* average lifetime in the *trans push−pull* systems (red dashed line, Figure 2f,g) is about three times longer than that in the *bending* paths (green dashed lines Figure 2f,g), which is again similar to the dynamics of *trans*-AB from the $n\pi^*$ state (62 vs 270 fs, Figure 2d,k). The longer lifetime of the *torsional versus bending* path could be simply referred to the time needed for internal vibrational energy redistribution from the *bending* to *torsional* mode, which is necessary to populate the MEP leading to the $n\pi^*$ decay process to the GS.[47] This is in line with the recently published AB $\pi\pi^*$ CASPT2 dynamics,[12] indicating that the productive CN═NC *torsional* mechanism is slower than the unproductive route characterized by symmetric *bending* modes.

To explain the opposite trend in the S_2 and S_1 lifetimes observed in *push−pull* AB as compared to the parent compound, we propose a simple model, which rationalizes entirely the differences documented in both ESs for the three systems. Because the *push−pull* substituents stabilize only the bright state, while keeping the $n\pi^*$ energy unaffected, we imagine a simple shift of the $\pi\pi^*$ PES, as shown in Scheme 2. By lowering the $\pi\pi^*$ state, the crossing with $n\pi^*$ becomes

https://dx.doi.org/10.1021/acs.jpca.0c08672
J. Phys. Chem. A 2020, 124, 9513−9523

Scheme 2. *Push–Pull* Substitution Effect

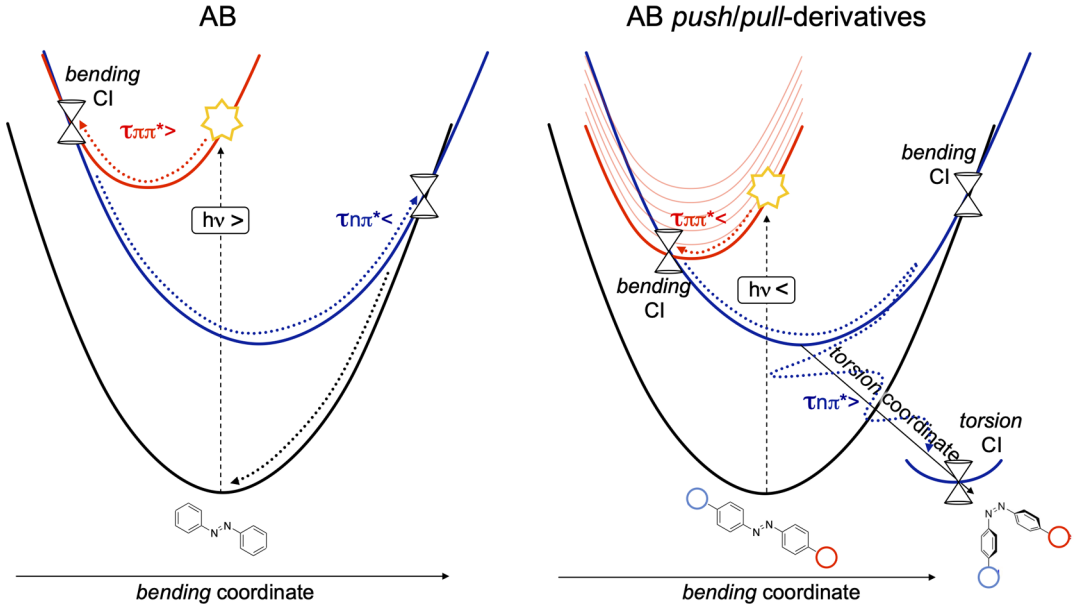

more accessible (*i.e.*, lower activation energy), thus leading to a shorter S_2 lifetime for the *push–pull* derivatives (Figure 2). Additionally, less energy becomes available along the initially populated bending modes on S_1 to eventually access the higher energy S_1/S_0 crossing region at roughly planar structures (torsional angle CNNC around 180°). Eventually, vibrational energy redistribution takes place, triggering population of the nπ^* (*torsional*) minimum energy path and populating the slower, but more productive, torsional paths leading to rotated S_1/S_0 CI structures.

***cis*-AB Systems.** *Cis*-isomers behave similarly to the *trans* ones: the *push–pull* substituents red-shift the $\pi\pi^*$ intense band according to their electron-donating/withdrawing strength, leaving the nπ^* state energy roughly unchanged (Table 1). The main difference with respect to the *trans*-conformers is that except for few outliers, more than 99% of the 120 *cis*-dynamics reach $S_1 \rightarrow S_0$ regions, which is always attributed to the CNNC *torsional* decay mechanism (CNNC > 45°; see Tables 2 and S7–S9 in the Supporting Information), as clearly shown in Figure 3. This is in line with the larger experimental QY observed in *cis*-AB (Φ = 0.27 vs 0.11 of the *trans*[29]). Moreover, *torsion* is activated already on S_2 (reaching torsion values up to 50°; see Figure 3) and becomes notably larger on the S_1, as shown by the torsion panels of Figure 4, because of the nonplanar FC starting structure. The earlier activation of the *torsional* motion, compared to the *trans* analogues, impedes the early decay to the nπ^* state through the *bending* funnel, resulting in longer S_2 lifetimes of the *cis*-isomers, compared to the *trans* ones, in agreement with previous dynamics simulations of AB from the $\pi\pi^*$ state.[52] The bending motions are more asymmetric than those in the *trans*-systems (Table 2), and to be more specific, the larger bendings are mainly attributed to the fragment bearing the electron donor group (−OMe or $-NH_2$; see Tables S8 and S9 in the Supporting Information). Anyways, none of the *cis*-dynamics reach bending angles close to 180° (see Tables S7–S9), suggesting that the *inversion* path is not populated, as already noted for *trans*-systems. The S_2 lifetime is shortening with the increasing *push–pull* strength (Figure 4a–c and g–i), supporting the previously explained hypothesis that the $\pi\pi^*$ red shift speeds up the access to the $\pi\pi^*/n\pi^*$ crossing seam (Scheme 2). Instead, the nπ^* lifetime in the *cis*-isomers is not affected by the *push–pull* substituents (Figure 4d–f and j–l) because the steeper gradient along the torsional coordinate drives the system straight to the rotated nπ^*/S_0 peaked CIs, as documented previously.[11,53] These differences in the S_1 PES shape (compared to the flat *trans*-nπ^* surface) correlate with a larger amount of kinetic energy along the torsional mode, inevitably leading to an increased photoisomerization QY with respect to the *trans* analogues.

That said, looking at the S_2/S_1 and S_1/S_0 CI distribution along the torsion/bending coordinates in Figure 3, we see that the parent and *push–pull*-derivatives behave similarly, populating the same photoisomerization processes and thus suggesting similar photoisomerization QYs (which is expected to remain higher than that in the *trans* analogues).

■ CONCLUSIONS

Kasha's rule violation in AB systems was often attributed to two different decay channels that are populated when exciting directly the $\pi\pi^*$ (S_2) or nπ^* (S_1) state. The present work supports and extends this hypothesis by proposing a unified mechanistic model, which can be applied to both azobenzene and its *push–pull* derivatives, foreseeing a higher QY for the latter, with respect to the parent compound. By analyzing a large number of TD-DFT (RASPT2 validated) $\pi\pi^*$ molecular dynamics on AB and two *push–pull* AB derivatives, we see that S_2 trajectories in the parent compound are mainly characterized by CNN/NNC bending motions preserving the system planarity and eventually leading to S_2/S_1 and, subsequently, to S_1/S_0 crossing regions, which are unproductive and drive the systems back to reactant repopulation. Indeed, only a small number of trajectories redistributes the vibrational energy along the *torsional* mode that could drive the system to the fully rotated S_1/S_0 CI (~90°), triggering the isomerization. We demonstrate that *push–pull* substituents mitigate this situation, leading to a behavior from the $\pi\pi^*$ state (bright) that is similar to that of the productive nπ^* state (dark). Indeed, the substituents induce a $\pi\pi^*$ red shift, bringing the bright state

https://dx.doi.org/10.1021/acs.jpca.0c08672
J. Phys. Chem. A 2020, 124, 9513–9523

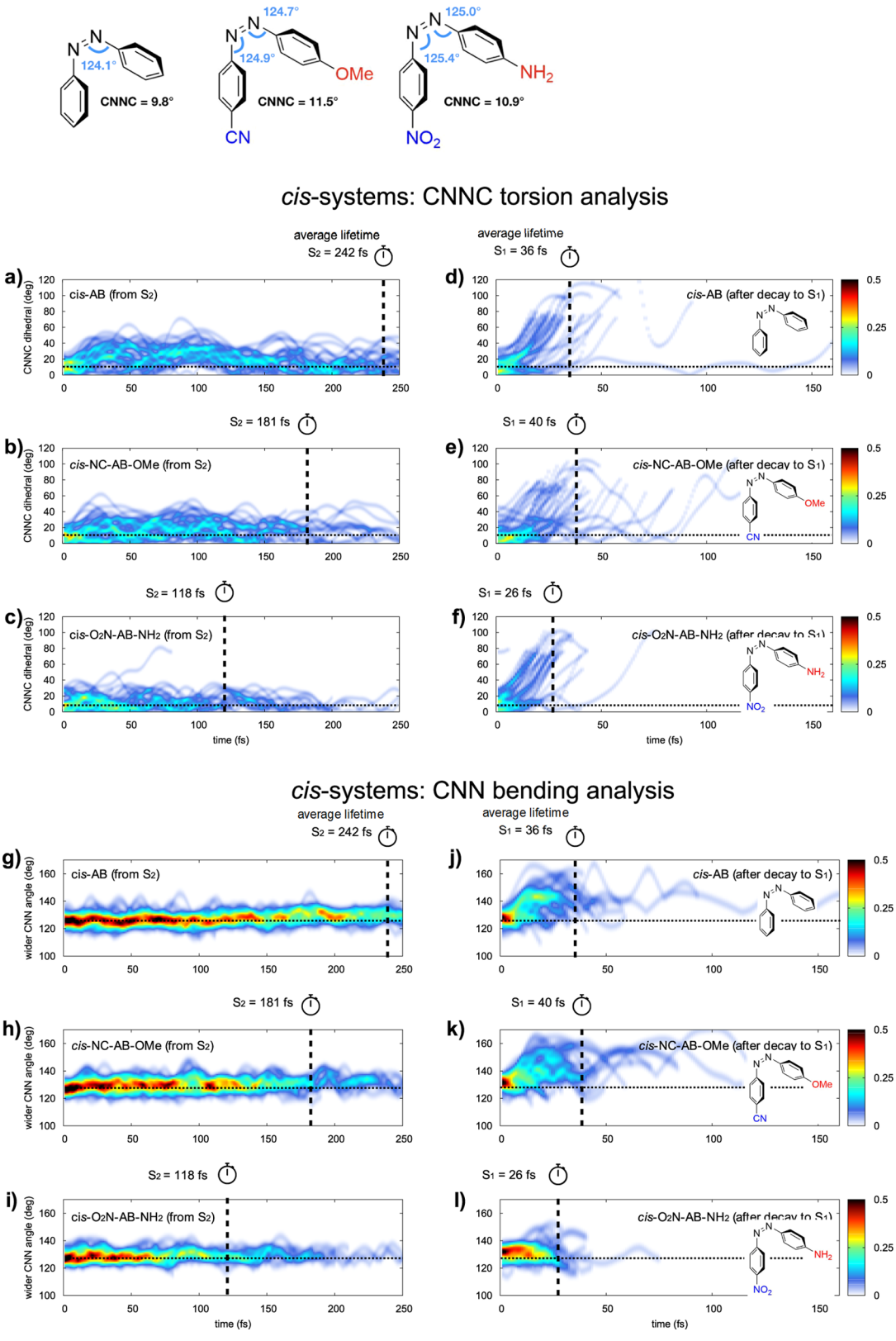

Figure 4. Normalized distribution of the CNNC *torsional* value (top panels) and widest CNN bending value (bottom panels) over time for the *cis*-system dynamics (40 for each panel) on S_2 (left) and on S_1 (right) until decay to the GS. The color scale refers to the normalized density of trajectories. Vertical dashed lines: ES lifetimes averaged over all trajectories. Horizontal dotted lines: FC value of the relative coordinate. Top left structures: CNNC torsion and CNN bending values in the S_0 minimum *cis*-systems (DFT/B3LYP/6-31G*-optimized).

closer to the dark nπ^* and therefore leading to the population of the same (and more productive) torsional pathways (Scheme 2). This demonstration, based on a significant number of trajectories, endorses the *push*−*pull* derivatives as flexible candidates for more efficient and visible light-activated switches, which are attractive for technological and biological

https://dx.doi.org/10.1021/acs.jpca.0c08672
J. Phys. Chem. A 2020, 124, 9513−9523

applications. Moreover, the large number of trajectories is a strong statistical support to finally assign the photoisomerization process exclusively to the torsion mechanism, even if it is assisted by large CNN/NNC bending motions.[11,12,14,48,53] Indeed, structures distorted enough to support a photoisomerization driven by the *inversion* route are never reached (Scheme 1). Therefore, only the *torsion* is the productive path, while the pure *bending* is an unproductive reaction coordinate, justifying the lower QY observed in AB when exciting the $\pi\pi^*$ state (*bending*-dominated) as compared to direct $n\pi^*$ excitation (*torsion*-driven). Because of the importance of the embedding on the excited-state dynamics,[54−56] QM/MM studies are currently undergoing to disclose effects of solvent polarity and viscosity on the photoactivity of these systems.

■ ASSOCIATED CONTENT

Supporting Information

The Supporting Information is available free of charge at https://pubs.acs.org/doi/10.1021/acs.jpca.0c08672.

Computational details, vertical excitation energies and dipole moments of AB *push*−*pull* derivatives, nature of TD-DFT and RASPT2 ESs, charge distribution in the FC geometry, details on TD-DFT dynamics, RASPT2 energies at S_1/S_0 crossings (0 K dynamics), and Cartesian coordinates of the B3LYP/DFT/6-31G*-optimized GS minima (PDF)

■ AUTHOR INFORMATION

Corresponding Authors

Marco Garavelli − *Dipartimento di Chimica Industriale "Toso Montanari", Università di Bologna, 40136 Bologna, Italy;* orcid.org/0000-0002-0796-289X; Email: marco.garavelli@unibo.it

Irene Conti − *Dipartimento di Chimica Industriale "Toso Montanari", Università di Bologna, 40136 Bologna, Italy;* orcid.org/0000-0001-7982-4480; Email: irene.conti@unibo.it

Authors

Flavia Aleotti − *Dipartimento di Chimica Industriale "Toso Montanari", Università di Bologna, 40136 Bologna, Italy*

Artur Nenov − *Dipartimento di Chimica Industriale "Toso Montanari", Università di Bologna, 40136 Bologna, Italy;* orcid.org/0000-0003-3071-5341

Luca Salvigni − *Dipartimento di Chimica Industriale "Toso Montanari", Università di Bologna, 40136 Bologna, Italy*

Matteo Bonfanti − *Dipartimento di Chimica Industriale "Toso Montanari", Università di Bologna, 40136 Bologna, Italy*

Mohsen M. El-Tahawy − *Dipartimento di Chimica Industriale "Toso Montanari", Università di Bologna, 40136 Bologna, Italy; Chemistry Department, Faculty of Science, Damanhour University, 22511 Damanhour, Egypt*

Andrea Giunchi − *Dipartimento di Chimica Industriale "Toso Montanari", Università di Bologna, 40136 Bologna, Italy*

Marziogiuseppe Gentile − *Dipartimento di Chimica "Giacomo Ciamician", Università di Bologna, 40126 Bologna, Italy*

Claudia Spallacci − *Dipartimento di Chimica Industriale "Toso Montanari", Università di Bologna, 40136 Bologna, Italy*

Alessia Ventimiglia − *Dipartimento di Chimica Industriale "Toso Montanari", Università di Bologna, 40136 Bologna, Italy*

Giuseppe Cirillo − *Dipartimento di Chimica Industriale "Toso Montanari", Università di Bologna, 40136 Bologna, Italy*

Lorenzo Montali − *Dipartimento di Chimica Industriale "Toso Montanari", Università di Bologna, 40136 Bologna, Italy*

Stefano Scurti − *Dipartimento di Chimica Industriale "Toso Montanari", Università di Bologna, 40136 Bologna, Italy*

Complete contact information is available at: https://pubs.acs.org/10.1021/acs.jpca.0c08672

Author Contributions

‖F.A. and A.N. contributed equally.

Funding

Financial support from the PHANTOMS project, PRIN: PROGETTI DI RICERCA DI RILEVANTE INTERESSE NAZIONALE − Bando 2017, Prot. 2017A4XRCA, is acknowledged. M.G., I.C., and A.N. acknowledge support from the H2020-NMBP-TO-IND-2018-2020/DT-NMBP-09-2018 project SIMDOME, grant agreement no. 814492.

Notes

The authors declare no competing financial interest.

■ REFERENCES

(1) Zimmerman, G.; Chow, L.-Y.; Paik, U.-J. The Photochemical Isomerization of Azobenzene. *J. Am. Chem. Soc.* **1958**, *80*, 3528−3531.

(2) Liu, Z. F.; Hashimoto, K.; Fujishima, A. Photoelectrochemical Information Storage Using an Azobenzene Derivative. *Nature* **1990**, *347*, 658−660.

(3) Hugel, T.; Holland, N. B.; Cattani, A.; Moroder, L.; Seitz, M.; Gaub, H. E. Single-Molecule Optomechanical Cycle. *Science* **2002**, *296*, 1103−1106.

(4) Chang, C.-W.; Lu, Y.-C.; Wang, T.-T.; Diau, E. W.-G. Photoisomerization Dynamics of Azobenzene in Solution with S_1 Excitation: A Femtosecond Fluorescence Anisotropy Study. *J. Am. Chem. Soc.* **2004**, *126*, 10109−10118.

(5) Schultz, T.; Quenneville, J.; Levine, B.; Toniolo, A.; Martínez, T. J.; Lochbrunner, S.; Schmitt, M.; Shaffer, J. P.; Zgierski, M. Z.; Stolow, A. Mechanism and Dynamics of Azobenzene Photoisomerization. *J. Am. Chem. Soc.* **2003**, *125*, 8098−8099.

(6) Casellas, J.; Bearpark, M. J.; Reguero, M. Excited State Decay in the Photoisomerization of Azobenzene: A New Balance between Mechanisms. *ChemPhysChem* **2016**, *17*, 3068.

(7) Henzl, J.; Mehlhorn, M.; Gawronski, H.; Rieder, K.-H.; Morgenstern, K. Reversible Cis−Trans Isomerization of a Single Azobenzene Molecule. *Angew. Chem., Int. Ed.* **2006**, *45*, 603−606.

(8) Bandara, H. M. D.; Burdette, S. C. Photoisomerization in Different Classes of Azobenzene. *Chem. Soc. Rev.* **2012**, *41*, 1809−1825.

(9) Fregoni, J.; Granucci, G.; Coccia, E.; Persico, M.; Corni, S. Manipulating Azobenzene Photoisomerization through Strong Light−Molecule Coupling. *Nat. Commun.* **2018**, *9*, 4688.

(10) Amirjalayer, S.; Buma, W. J. Light on the Structural Evolution of Photoresponsive Molecular Switches in Electronically Excited States. *Chem.—Eur. J.* **2019**, *25*, 6252−6258.

(11) Conti, I.; Garavelli, M.; Orlandi, G. The Different Photoisomerization Efficiency of Azobenzene in the Lowest $n\pi^*$ and $\pi\pi^*$ Singlets: The Role of a Phantom State. *J. Am. Chem. Soc.* **2008**, *130*, 5216−5230.

(12) Nenov, A.; Borrego-Varillas, R.; Oriana, A.; Ganzer, L.; Segatta, F.; Conti, I.; Segarra-Marti, J.; Omachi, J.; Dapor, M.; Taioli, S.; Manzoni, C.; Mukamel, S.; Cerullo, G.; Garavelli, M. UV-Light-

Induced Vibrational Coherences: The Key to Understand Kasha Rule Violation in *trans*-Azobenzene. *J. Phys. Chem. Lett.* **2018**, *9*, 1534−1541.
(13) Tan, E. M. M.; Amirjalayer, S.; Smolarek, S.; Vdovin, A.; Zerbetto, F.; Buma, W. J. Fast Photodynamics of Azobenzene Probed by Scanning Excited-State Potential Energy Surfaces Using Slow Spectroscopy. *Nat. Commun.* **2015**, *6*, 5860.
(14) Conti, I.; Marchioni, F.; Credi, A.; Orlandi, G.; Rosini, G.; Garavelli, M. Cyclohexenylphenyldiazene: A Simple Surrogate of the Azobenzene Photochromic Unit. *J. Am. Chem. Soc.* **2007**, *129*, 3198−3210.
(15) Browne, W. R.; Feringa, B. L. Chiroptical Molecular Switches. In *Molecular Switches*; Feringa, B. L., Browne, W. R., Eds.; Wiley-VCH: Weinheim, Germany, 2011; pp 121−179.
(16) Crespi, S.; Simeth, N. A.; König, B. Heteroaryl Azo Dyes as Molecular Photoswitches. *Nat. Rev. Chem.* **2019**, *3*, 133−146.
(17) Mativetsky, J. M.; Pace, G.; Elbing, M.; Rampi, M. A.; Mayor, M.; Samorì, P. Azobenzenes as Light-Controlled Molecular Electronic Switches in Nanoscale Metal−Molecule−Metal Junctions. *J. Am. Chem. Soc.* **2008**, *130*, 9192−9193.
(18) Marturano, V.; Ambrogi, V.; Bandeira, N. A. G.; Tylkowski, B.; Giamberini, M.; Cerruti, P. Modeling of Azobenzene-Based Compounds. *Phys. Sci. Rev.* **2017**, *2*, 20170138 DOI: 10.1515/psr-2017-0138.
(19) Sadovski, O.; Beharry, A. A.; Zhang, F.; Woolley, G. A. Spectral Tuning of Azobenzene Photoswitches for Biological Applications. *Angew. Chem., Int. Ed.* **2009**, *48*, 1484−1486.
(20) Beharry, A. A.; Woolley, G. A. Azobenzene Photoswitches for Biomolecules. *Chem. Soc. Rev.* **2011**, *40*, 4422−4437.
(21) Ikeda, T.; Tsutsumi, O. Optical Switching and Image Storage by Means of Azobenzene Liquid-Crystal Films. *Science* **1995**, *268*, 1873−1875.
(22) Zhang, C.; Du, M.-H.; Cheng, H.-P.; Zhang, X.-G.; Roitberg, A. E.; Krause, J. L. Coherent Electron Transport through an Azobenzene Molecule: A Light-Driven Molecular Switch. *Phys. Rev. Lett.* **2004**, *92*, 158301.
(23) Muraoka, T.; Kinbara, K.; Kobayashi, Y.; Aida, T. Light-Driven Open−Close Motion of Chiral Molecular Scissors. *J. Am. Chem. Soc.* **2003**, *125*, 5612−5613.
(24) Renner, C.; Moroder, L. Azobenzene as Conformational Switch in Model Peptides. *ChemBioChem* **2006**, *7*, 868−878.
(25) Volgraf, M.; Gorostiza, P.; Numano, R.; Kramer, R. H.; Isacoff, E. Y.; Trauner, D. Allosteric Control of an Ionotropic Glutamate Receptor with an Optical Switch. *Nat. Chem. Biol.* **2006**, *2*, 47−52.
(26) Bose, M.; Groff, D.; Xie, J.; Brustad, E.; Schultz, P. G. The Incorporation of a Photoisomerizable Amino Acid into Proteins in E. Coli. *J. Am. Chem. Soc.* **2006**, *128*, 388−389.
(27) Fortin, D. L.; Banghart, M. R.; Dunn, T. W.; Borges, K.; Wagenaar, D. A.; Gaudry, Q.; Karakossian, M. H.; Otis, T. S.; Kristan, W. B.; Trauner, D.; Kramer, R. H. Photochemical Control of Endogenous Ion Channels and Cellular Excitability. *Nat. Methods* **2008**, *5*, 331−338.
(28) Andersson, J.-Å.; Petterson, R.; Tegnér, L. Flash Photolysis Experiments in the Vapour Phase at Elevated Temperatures I: Spectra of Azobenzene and the Kinetics of Its Thermal Cis−Trans Isomerization. *J. Photochem.* **1982**, *20*, 17−32.
(29) Bortolus, P.; Monti, S. Cis−Trans Photoisomerization of Azobenzene. Solvent and Triplet Donors Effects. *J. Phys. Chem.* **1979**, *83*, 648−652.
(30) Dong, M.; Babalhavaeji, A.; Samanta, S.; Beharry, A. A.; Woolley, G. A. Red-Shifting Azobenzene Photoswitches for In Vivo Use. *Acc. Chem. Res.* **2015**, *48*, 2662−2670.
(31) Fregoni, J.; Granucci, G.; Coccia, E.; Persico, M.; Corni, S. Manipulating Azobenzene Photoisomerization through Strong Light−Molecule Coupling. *Nat. Commun.* **2018**, *9*, 4688.
(32) Rashid, M. A. M.; Hayati, D.; Kwak, K.; Hong, J. Computational Investigation of Tuning the Electron-Donating Ability in Metal-Free Organic Dyes Featuring an Azobenzene Spacer for Dye-Sensitized Solar Cells. *Nanomaterials* **2019**, *9*, 119.
(33) Crecca, C. R.; Roitberg, A. E. Theoretical Study of the Isomerization Mechanism of Azobenzene and Disubstituted Azobenzene Derivatives. *J. Phys. Chem. A* **2006**, *110*, 8188−8203.
(34) Satzger, H.; Root, C.; Braun, M. Excited-State Dynamics of *trans*- and *cis*-Azobenzene after UV Excitation in the $\pi\pi^*$ Band. *J. Phys. Chem. A* **2004**, *108*, 6265−6271.
(35) Zhao, C.; Horiuchi, H.; Hoshi, T.; Hasegawa, M.; Kobayashi, M.; Hiratsuka, H. Observation of the Radical Anion Intermediates in the Photolyses of 4-Cyano- and 4-Nitro-Azobenzene in MTHF at 77 K. *Chem. Lett.* **2003**, *32*, 124−125.
(36) Rodionova, G. N.; Krutovskaya, I. V.; Tuchin, Y. G.; Rodionov, A. N.; Karpov, V. V. Electronic Spectra and Structure of Several Azo Dyes in Various States of Aggregation. *J. Appl. Spectrosc.* **1981**, *34*, 434−438.
(37) Kobayashi, S.; Yokoyama, H.; Kamei, H. Substituent and Solvent Effects on Electronic Absorption Spectra and Thermal Isomerization of Push−Pull-Substituted *cis*-Azobenzenes. *Chem. Phys. Lett.* **1987**, *138*, 333−338.
(38) Masoud, M. S.; Ali, A. E.; Shaker, M. A.; Ghani, M. A. Solvatochromic Behavior of the Electronic Absorption Spectra of Some Azo Derivatives of Amino Pyridines. *Spectrochim. Acta Mol. Biomol. Spectrosc.* **2004**, *60*, 3155−3159.
(39) Airinei, A.; Homocianu, M.; Dorohoi, D. O. Changes Induced by Solvent Polarity in Electronic Absorption Spectra of Some Azo Disperse Dyes. *J. Mol. Liq.* **2010**, *157*, 13−17.
(40) Gabor, G.; Fischer, E. Spectra and Cis−Trans Isomerism in Highly Dipolar Derivatives of Azobenzene. *J. Phys. Chem.* **1971**, *75*, 581−583.
(41) Yamada, S.; Bessho, J.; Nakasato, H.; Tsutsumi, O. Color Tuning Donor−Acceptor-Type Azobenzene Dyes by Controlling the Molecular Geometry of the Donor Moiety. *Dyes Pigments* **2018**, *150*, 89−96.
(42) Krawczyk, P. DFT Study of Linear and Nonlinear Optical Properties of Donor−Acceptor Substituted Stilbenes, Azobenzenes and Benzilideneanilines. *J. Mol. Model.* **2010**, *16*, 659−668.
(43) Liu, J.-n.; Chen, Z.-r.; Yuan, S.-f. Study on the Prediction of Visible Absorption Maxima of Azobenzene Compounds. *J. Zhejiang Univ., Sci.* **2005**, *6B*, 584−589.
(44) Blevins, A. A.; Blanchard, G. J. Effect of Positional Substitution on the Optical Response of Symmetrically Disubstituted Azobenzene Derivatives. *J. Phys. Chem. B* **2004**, *108*, 4962−4968.
(45) Antonov, L.; Kamada, K.; Ohta, K.; Kamounah, F. S. A Systematic Femtosecond Study on the Two-Photon Absorbing D-π-A Molecules−π-Bridge Nitrogen Insertion and Strength of the Donor and Acceptor Groups. *Phys. Chem. Chem. Phys.* **2003**, *5*, 1193−1197.
(46) García-Amorós, J.; Velasco, D. Recent Advances towards Azobenzene-Based Light-Driven Real-Time Information-Transmitting Materials. *Beilstein J. Org. Chem.* **2012**, *8*, 1003−1017.
(47) Aleotti, F.; Soprani, L.; Nenov, A.; Berardi, R.; Arcioni, A.; Zannoni, C.; Garavelli, M. Multidimensional Potential Energy Surfaces Resolved at the RASPT2 Level for Accurate Photoinduced Isomerization Dynamics of Azobenzene. *J. Chem. Theory Comput.* **2019**, *15*, 6813−6823.
(48) Ciminelli, C.; Granucci, G.; Persico, M. The Photoisomerization Mechanism of Azobenzene: A Semiclassical Simulation of Nonadiabatic Dynamics. *Chem.—Eur. J.* **2004**, *10*, 2327−2341.
(49) Granucci, G.; Persico, M. Excited State Dynamics with the Direct Trajectory Surface Hopping Method: Azobenzene and Its Derivatives as a Case Study. *Theor. Chem. Acc.* **2007**, *117*, 1131−1143.
(50) Toniolo, A.; Ciminelli, C.; Persico, M.; Martínez, T. J. Simulation of the Photodynamics of Azobenzene on Its First Excited State: Comparison of Full Multiple Spawning and Surface Hopping Treatments. *J. Chem. Phys.* **2005**, *123*, 234308.
(51) Tiberio, G.; Muccioli, L.; Berardi, R.; Zannoni, C. How Does the Trans−Cis Photoisomerization of Azobenzene Take Place in Organic Solvents? *ChemPhysChem* **2010**, *11*, 1018−1028.
(52) Cantatore, V.; Granucci, G.; Persico, M. Simulation of the $\pi\rightarrow\pi^*$ Photodynamics of Azobenzene: Decoherence and Solvent Effects. *Comput. Theor. Chem.* **2014**, *1040−1041*, 126−135.

(53) Cembran, A.; Bernardi, F.; Garavelli, M.; Gagliardi, L.; Orlandi, G. On the Mechanism of the Cis−Trans Isomerization in the Lowest Electronic States of Azobenzene: S_0, S_1, and T_1. *J. Am. Chem. Soc.* **2004**, *126*, 3234−3243.
(54) Conti, I.; Garavelli, M. Evolution of the Excitonic State of DNA Stacked Thymines: Intrabase $\pi\pi^* \rightarrow S_0$ Decay Paths Account for Ultrafast (Subpicosecond) and Longer (>100 Ps) Deactivations. *J. Phys. Chem. Lett.* **2018**, *9*, 2373−2379.
(55) Teles-Ferreira, D. C.; Conti, I.; Borrego-Varillas, R.; Nenov, A.; Van Stokkum, I. H. M.; Ganzer, L.; Manzoni, C.; Paula, A. M.; Cerullo, G.; Garavelli, M. A Unified Experimental/Theoretical Description of the Ultrafast Photophysics of Single and Double Thionated Uracils. *Chem.—Eur. J.* **2020**, *26*, 336−343.
(56) Nenov, A.; Conti, I.; Borrego-Varillas, R.; Cerullo, G.; Garavelli, M. Linear absorption spectra of solvated thiouracils resolved at the hybrid RASPT2/MM level. *Chem. Phys.* **2018**, *515*, 643−653.

NOTE ADDED AFTER ASAP PUBLICATION

This article published November 10, 2020 with an error in Scheme 2. The corrected file published November 19, 2020.

https://dx.doi.org/10.1021/acs.jpca.0c08672
J. Phys. Chem. A 2020, 124, 9513−9523